

Article

# Waxberry-Like Nanosphere $\text{Li}_4\text{Mn}_5\text{O}_{12}$ as High Performance Electrode Materials for Supercapacitors

Peiyuan Ji <sup>1</sup>, Yi Xi <sup>1,2,3,\*</sup>, Chengshuang Zhang <sup>1,2,3</sup>, Chuanshen Wang <sup>1</sup>, Chenguo Hu <sup>1</sup>, Yuzhu Guan <sup>1</sup> and Dazhi Zhang <sup>1,\*</sup>

<sup>1</sup> Department of Applied Physics, State Key Laboratory of Power Transmission Equipment & System Security and New Technology, Chongqing University, Chongqing 400044, China; 20162702008@cqu.edu.cn (P.J.); 20152702027@cqu.edu.cn (C.Z.); 20182701014@cqu.edu.cn (C.W.); hucg@cqu.edu.cn (C.H.); 20172702002t@cqu.edu.cn (Y.G.)

<sup>2</sup> CAS Center for Excellence in Nanoscience, Beijing Institute of Nanoenergy and Nanosystems Chinese Academy of Sciences, Beijing 100083, China

<sup>3</sup> College of Nanoscience and Technology, University of Chinese Academy of Sciences, Beijing 100049, China

\* Correspondence: yxi6@cqu.edu.cn (Y.X.); dazhi.zhang@163.com (D.Z.)

Received: 13 June 2018; Accepted: 4 September 2018; Published: 11 September 2018



**Abstract:** Porous materials have superior electrochemical performance owing to its their structure, which could increase the specific and contact area with the electrode. The spinel  $\text{Li}_4\text{Mn}_5\text{O}_{12}$  has a three-dimensional tunnel structure for a better diffusion path, which has the advantage of lithium ion insertion and extraction in the framework. However, multi-space spherical materials with single morphologies are rarely studied. In this work, waxberry-like and raspberry-like nanospheres for  $\text{Li}_4\text{Mn}_5\text{O}_{12}$  have been fabricated by the wet chemistry and solid-state methods for the first time. The diameter of a single waxberry- and raspberry-like nanosphere is about 1  $\mu\text{m}$  and 600 nm, respectively. The specific capacitance of  $\text{Li}_4\text{Mn}_5\text{O}_{12}$  was 535  $\text{mF cm}^{-2}$  and 147.25  $\text{F g}^{-1}$  at the scan rate of 2  $\text{mV s}^{-1}$ , and the energy density was 110.7  $\text{Wh kg}^{-1}$ , remaining at 70% after 5000th charge-discharge cycles. Compared with raspberry-like nanosphere  $\text{Li}_4\text{Mn}_5\text{O}_{12}$ , the waxberry-like nanoporous spinel  $\text{Li}_4\text{Mn}_5\text{O}_{12}$  shows the better electrochemical performance and stability; furthermore, these electrochemical performances have been improved greatly compared to the previous studies. All these results indicate that the waxberry-like nanoporous spinel  $\text{Li}_4\text{Mn}_5\text{O}_{12}$  could provide a potential application in high performance supercapacitors.

**Keywords:** supercapacitors;  $\text{Li}_4\text{Mn}_5\text{O}_{12}$ ; waxberry-like nanosphere; high performance

## 1. Introduction

With the development of global economy and the progress of science and technology, more and more electronic products come to enter the human life. These electronic products provide great help and support for the development of human beings and the progress of science and technology, which improve the level of development of productive social forces greatly. However, for most electronic devices, their operation is inseparable from the supply of energy systems. Nowadays, almost all of the energy supply of electronic equipment is dominated by electricity. In particular, micro energy storage devices are integrated into small- and medium-sized electronic devices, as well as energy storage systems in portable electronic devices; most of these energy storage devices are batteries based on lithium ions, which were widely used due to their high energy density, wide charging voltage, and long discharging time [1]. Although lithium batteries have a wide range of applications in society, due to some unsatisfactory aspects on lithium battery, such as the lower rate capability, reliability, cycling life, and power density [2], seeking high performance storage devices and their electrode materials have

become a main problem in some areas of development for science and technology. In recent years, supercapacitors have gained much more attention, due to their superior cycling life, high power density, safety, low cost, stability, and so on [3–5]. One of main storage performance factors for supercapacitors is the electrode materials. The different micro or nano-structure lithium manganese materials, such as  $\text{LiMn}_2\text{O}_4$ ,  $\text{Li}_2\text{MnO}_3$ , and  $\text{Li}_4\text{Mn}_5\text{O}_{12}$ , were widely studied as an anode material, owing to their superior electrical performance [1,6–15]. The different structure and morphology of electrode materials produce an effect on the performance of the storage device. The porous  $\text{LiMn}_2\text{O}_4$  shows the excellent cycling performance at the rate of 9 C ( $1000 \text{ mA g}^{-1}$ ) and good stability [2].  $\text{Li}_4\text{Mn}_5\text{O}_{12}$  nano-crystallites exhibit an excellent specific capacitance ( $200 \text{ F g}^{-1}$ ) and a high specific capacity ( $76 \text{ mAh g}^{-1}$ ) [16]. However,  $\text{Li}_4\text{Mn}_5\text{O}_{12}$  with uniform morphology and a good cycling stability was rarely synthesized and reported; at the same time,  $\text{Li}_4\text{Mn}_5\text{O}_{12}$  with waxberry-like nanosphere morphology as an electrode material for the supercapacitors and the mechanism of the storage was rarely studied as well. In order to synthesize new morphologies of  $\text{Li}_4\text{Mn}_5\text{O}_{12}$  and its electrochemical performance, we reported a method that uses the  $\text{Mn}_2\text{O}_3$  or  $\text{MnO}_2$  as the template. Waxberry-like and raspberry-like nanosphere  $\text{Li}_4\text{Mn}_5\text{O}_{12}$  was synthesized based on the structure of manganese oxide. Waxberry-like nanosphere  $\text{Li}_4\text{Mn}_5\text{O}_{12}$  has good electrochemical performance and cycle stability, due to its high crystalline and special structure.

## 2. Material and Methods

Some chemicals were used in the experiments, as follows: manganese (II) chloride tetra hydrate ( $\text{MnCl}_2 \cdot 4\text{H}_2\text{O}$ , Analytical Reagent Shanghai Aladdin Biochemical Technology Co., Ltd., Shanghai, China), sodium bicarbonate ( $\text{NaHCO}_3$ , Analytical Reagent Shanghai Aladdin Biochemical Technology Co., Ltd., Shanghai, China), and lithium hydroxide ( $\text{LiOH} \cdot \text{H}_2\text{O}$ , Analytical Reagent Shanghai Aladdin Biochemical Technology Co., Ltd., Shanghai, China). All chemicals had purity higher than 99.99% and were directly used without further purification.

### 2.1. Synthesis of Sphere $\text{MnCO}_3$

The  $\text{MnCO}_3$  microspheres were prepared by a modified precipitation method from a prior report [17]. Firstly, 1.682 g  $\text{NaHCO}_3$  was dissolved in 80 mL water under vigorous stirring which was named solution A. Secondly, 3.167 g  $\text{MnCl}_2 \cdot 4\text{H}_2\text{O}$  and 8 mL ethanol were dissolved in the other 80 mL water and stirred for 10 min, which was named solution B. Finally, solution A and B were mixed together under constant stirring for at least 1 h. The product was filtered and dried in a vacuum at  $60^\circ\text{C}$  for all night. The pink precipitate  $\text{MnCO}_3$  was finally obtained.

#### 2.1.1. Synthesis of Waxberry-Like Nanosphere $\text{Mn}_2\text{O}_3$

The as-obtained  $\text{MnCO}_3$  was loaded in a ceramic crucible and heated in a tube furnace under the temperature of  $550^\circ\text{C}$  for 6 h at the rate at  $2^\circ\text{C min}^{-1}$ . The black powder was directly obtained after heating treatment.

#### 2.1.2. Synthesis of $\alpha\text{-MnO}_2$

The prepared  $\alpha\text{-MnO}_2$  was obtained by a previously-listed method [18]. In a typical process, 40 mL  $\text{KMnO}_4$  ( $0.1 \text{ mol L}^{-1}$ ) and  $\text{MnSO}_4 \cdot 4\text{H}_2\text{O}$  ( $0.15 \text{ mol L}^{-1}$ ) were mixed together with constant stirring for 6 h. The dark precipitate was filtered and washed with ethanol and deionized water several times. The finally product was collected and dried in vacuum at  $70^\circ\text{C}$  for 12 h.

#### 2.1.3. Synthesis of Waxberry-Like Nanosphere and Raspberry-Like Nanosphere $\text{Li}_4\text{Mn}_5\text{O}_{12}$

The as-prepared  $\text{Mn}_2\text{O}_3/\alpha\text{-MnO}_2$  and  $\text{LiOH} \cdot \text{H}_2\text{O}$  were mixed together at the stoichiometric ratio of 5:8/5:4 in the water and 10 mL of ethanol. The mixed solution was stirred and dried under the

temperature at 50 °C. Then, the dried powder was loaded in a ceramic crucible and heated at 600 °C for 6 h with the rate of 2 °C min<sup>-1</sup>. The final black product Li<sub>4</sub>Mn<sub>5</sub>O<sub>12</sub> was obtained.

The morphology, formation mechanism, and synthesis method of Li<sub>4</sub>Mn<sub>5</sub>O<sub>12</sub> are shown in the Figure 1. Firstly, the Mn<sup>+</sup> and CO<sub>3</sub><sup>2-</sup> ions in the solution combine to form the MnCO<sub>3</sub> nanosphere at room temperature, and the MnCO<sub>3</sub> nanosphere then forms a porous manganese oxide nanosphere with a porous structure at 550 °C. The obtained nanosphere was put into the solution with sufficient contact with LiOH. Finally, the materials after drying at room temperature were heated at 600 °C in tube furnace to form the waxberry-like nanosphere Li<sub>4</sub>Mn<sub>5</sub>O<sub>12</sub>.

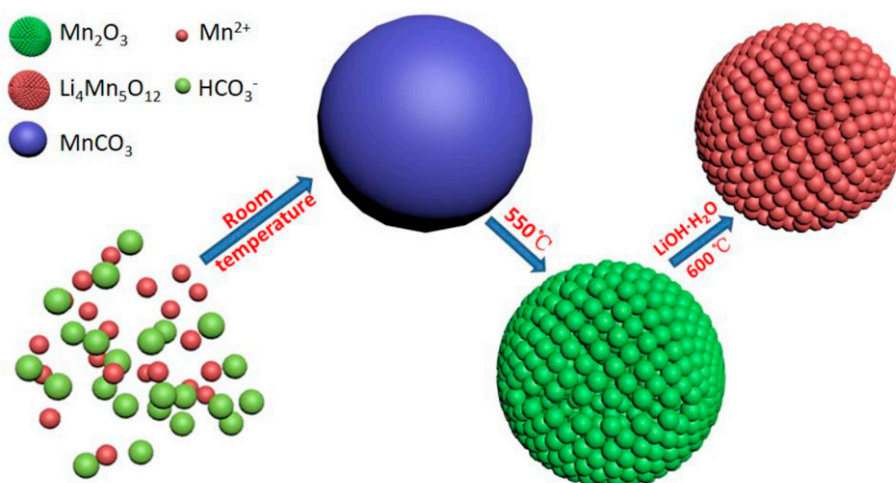


**Figure 1.** The synthesis mechanism of Li<sub>4</sub>Mn<sub>5</sub>O<sub>12</sub> under micro-scale.

## 2.2. Assembly of the Working Electrode

The working electrode was fabricated as follows. Firstly, the prepared Li<sub>4</sub>Mn<sub>5</sub>O<sub>12</sub> powder (both nanosphere and raspberry-like nanosphere Li<sub>4</sub>Mn<sub>5</sub>O<sub>12</sub>) was mixed with carbon black and polytetra-fluorene-ethylene (PTFE) binder with a mass ratio at 80:15:5 in 5 mL of ethanol. The mixed slurry was directly painted onto a carbon cloth (6 cm × 2 cm) and dried in the vacuum at 60 °C for 24 h to remove the ethanol on the electrode [4,19,20]. Secondly, the carbon cloth was then cut into three parts (2 cm × 2 cm each) after drying. Finally, the electrode holder was used to clamp the prepared individual electrode and directly immerse it into the 1 mol L<sup>-1</sup> LiNO<sub>3</sub> solution as the working electrode for the characterization and measurement in the three-electrode system. The Pt (platinum) and the Ag/AgCl electrodes were used as the opposite electrode and reference electrode, respectively.

## 2.3. Characterization and Measurement

The surface morphologies and structural properties of the products were characterized by field-emission scanning electron microscopy (JEOL JSM-7800F, Japanese electronics JEOL, Tokyo, Japan), X-ray diffraction (XRD, BDX3200 China with CuK<sub>α</sub> radiation), and transmission electron microscopy (TEM, TECNAI20, Philips, Amsterdam, Holland). The chemical workstation (CHI660e, Chenhua, Shanghai, China) was used for the measurement of the galvanostatic cycling (GCD), cyclic voltammeter (CV), and electrochemical impedance spectroscopy (EIS) about the working electrode.

# 3. Result and Discussion

## 3.1. Material Characterization

Figure 2a,b,e,f shows the SEM images of porous- and hollow-nanosphere Li<sub>4</sub>Mn<sub>5</sub>O<sub>12</sub>. The porous nanosphere looks like a waxberry, so it called “waxberry-like” nanosphere Li<sub>4</sub>Mn<sub>5</sub>O<sub>12</sub> (WLN), and the hollow nanosphere Li<sub>4</sub>Mn<sub>5</sub>O<sub>12</sub> looks like a raspberry, so it called “raspberry-like” nanosphere

$\text{Li}_4\text{Mn}_5\text{O}_{12}$  (RLN). As can be seen in the images, the two prepared samples showed uniform morphology and diameter; the radius of the waxberry-like nanosphere and raspberry-like nanosphere  $\text{Li}_4\text{Mn}_5\text{O}_{12}$  were about 500 nm and 300 nm, respectively. More surface details of two samples were further identified through high magnification, shown in Figure 2c,d,g,h. It can be seen that the surfaces of raspberry-like nanosphere  $\text{Li}_4\text{Mn}_5\text{O}_{12}$  (Figure 2c,d) contains the nanosheet structure and is not smooth, and the surface of the waxberry-like nanosphere  $\text{Li}_4\text{Mn}_5\text{O}_{12}$  (Figure 2g,h) also shows the unsmooth surface containing the porous structure that was assembled by a lot of smaller nanospheres. The waxberry-like nanosphere  $\text{Li}_4\text{Mn}_5\text{O}_{12}$  consists of many small  $\text{Li}_4\text{Mn}_5\text{O}_{12}$  balls that have unsmooth surfaces and multiple pores—the result corresponds to the SEM image above. It is worth noting that the morphologies of waxberry-like nanosphere and raspberry-like nanosphere  $\text{Li}_4\text{Mn}_5\text{O}_{12}$  had not been attained by the simple methods reported before [1,16,21–25]. The distribution of elements in the material is characterized by mapping, which was shown in Figure S1. Those elemental mapping studies further confirmed the homogeneously distributed O and Mn elements, both in the waxberry-like nanosphere  $\text{Li}_4\text{Mn}_5\text{O}_{12}$  Figure S1a–d and raspberry-like nanosphere  $\text{Li}_4\text{Mn}_5\text{O}_{12}$  (Figure S1e–h).

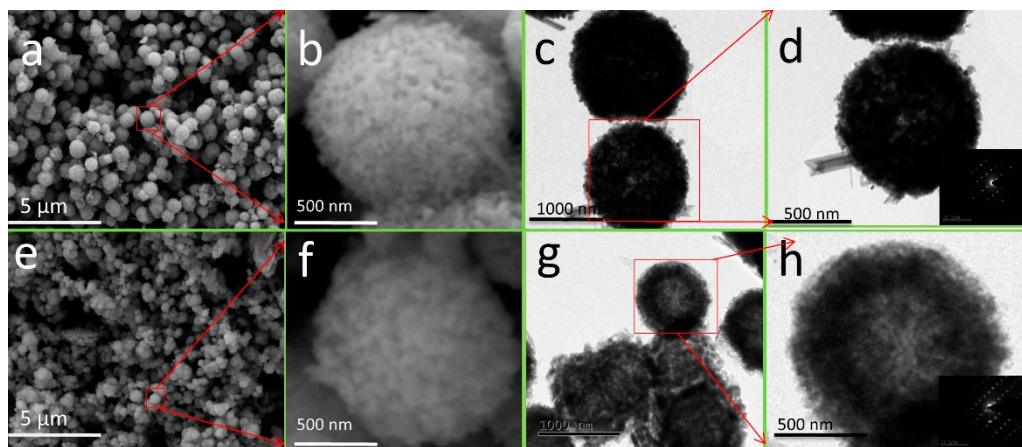


**Figure 2.** SEM images (a,b) and TEM images (c,d) of waxberry-like nanosphere  $\text{Li}_4\text{Mn}_5\text{O}_{12}$ . SEM images (e,f) and TEM images (g,h) of raspberry-like nanosphere  $\text{Li}_4\text{Mn}_5\text{O}_{12}$ .

Figure 3a shows the XRD pattern of raspberry-like nanosphere and waxberry-like nanosphere  $\text{Li}_4\text{Mn}_5\text{O}_{12}$ . After heating treatment at 600 °C, both of the samples showed the same diffraction peaks in the XRD patterns, which can be assigned to a pure phase of well-crystallized spinel structure  $\text{Li}_4\text{Mn}_5\text{O}_{12}$  that belongs to the  $Fd\bar{3}m$  space group (JCPDS: No. 46-0810) [1]. The small redundant peaks were considered to be  $\text{Mn}_2\text{O}_3$ ; due to the absence of reaction during the synthesis of  $\text{Li}_4\text{Mn}_5\text{O}_{12}$  at 600 °C, the  $\text{MnO}_2$  turn into  $\text{Mn}_2\text{O}_3$  in the process above [26]. Figure 3b,c reveals the spectra of energy dispersive spectroscopy (EDS) of the two samples. Both spectra demonstrate that the samples contain manganese and oxygen, which are in agreement with the XRD patterns [27]. The reason for lacking the Li peaks could be explained as follows: the window of EDS is usually made of beryllium, and the characteristic X-ray produced by elements below atomic number 11 is significantly absorbed. Therefore, elements with a small atomic number are not suitable for EDS measurement.

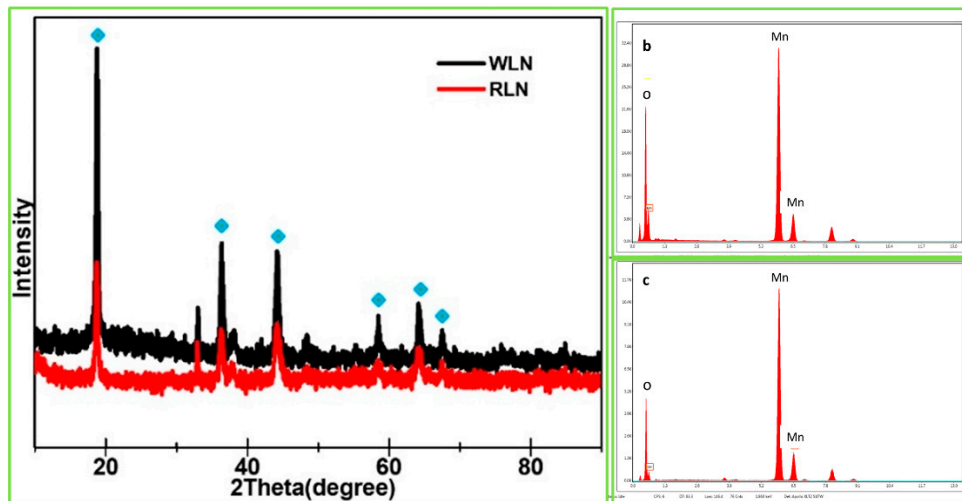


**Figure 3.** XRD (a), XPS (b) images of waxberry-like nanosphere  $\text{Li}_4\text{Mn}_5\text{O}_{12}$  and raspberry-like nanosphere  $\text{Li}_4\text{Mn}_5\text{O}_{12}$  (c).

### 3.2. Electrochemical Test

Here we will mainly study the electrochemical performance of WLN. The current of galvanostatic cycling was 10 mA with the potential range of 0–1 V. The potential windows of the CV were 0–1 V with different scan rates at 2, 5, 10, 20, 30, 40, 50, and 100 mV, respectively. The frequency of EIS was 0.01–10,000 Hz. The specific capacitance of the  $\text{Li}_4\text{Mn}_5\text{O}_{12}$  was calculated by the following equations [28,29].

$$E = \int U dQ = \int UI dt = IS \tag{1}$$

$$P = \frac{I \Delta V}{2m} \tag{2}$$

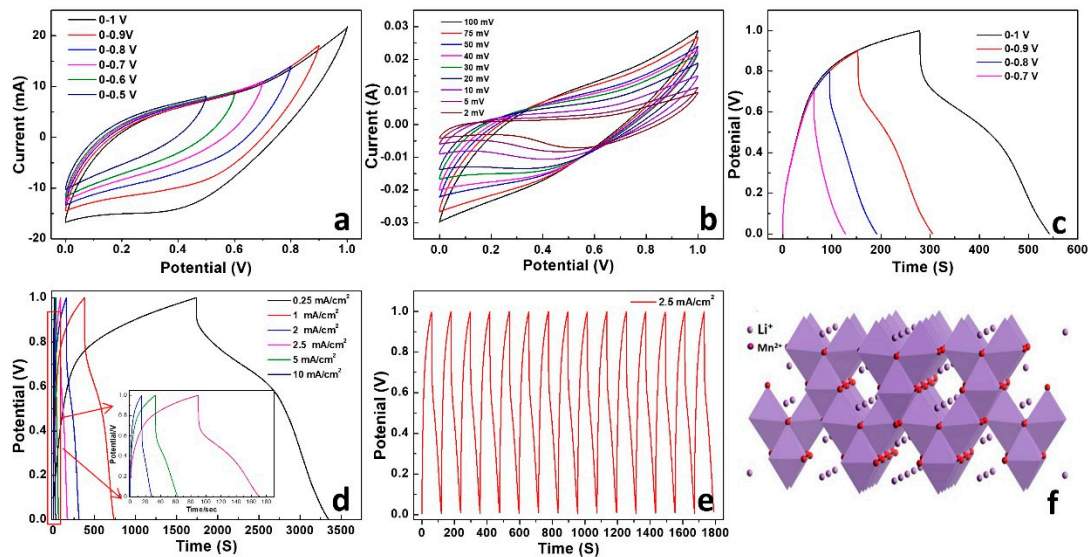
$$C_s = \frac{I \Delta t}{S \Delta v} C \tag{3}$$

$$C_m = \frac{1}{\Delta V (dV/dt)} \int I dV \tag{4}$$

where the  $E$  ( $\text{Wh kg}^{-1}$ ) is the energy density;  $P$  ( $\text{W kg}^{-1}$ ) is the power density;  $V_1$  and  $V_2$  are the end-of-charge voltage and the end-of-discharge voltage, respectively;  $C_s$  ( $\text{mF cm}^{-2}$ ) is the specific capacitance;  $C_m$  is the integral capacitance of the electrode, calculated from the CV curves;  $dV/dt$  is the voltage scan rate;  $m$  (g) is the mass of the  $\text{Li}_4\text{Mn}_5\text{O}_{12}$  loaded on the working electrode;  $S$  ( $\text{cm}^2$ ) is the area of the measured single electrode;  $I$  (A) is the current on the charge and discharge procession;  $\Delta t$  (s) is the discharging time; and  $\Delta v$  (V) is the potential window.

Figure 4a shows the CV image of waxberry-like nanosphere  $\text{Li}_4\text{Mn}_5\text{O}_{12}$  in  $1 \text{ mol L}^{-1} \text{ LiNO}_3$  electrolyte with the scan rate at  $20 \text{ mV s}^{-1}$  in a different potential window. Figure 4b displays the CV image of waxberry-like nanosphere  $\text{Li}_4\text{Mn}_5\text{O}_{12}$  in  $1 \text{ mol L}^{-1} \text{ LiNO}_3$  electrolyte with different scan rates; the cut-off range was chosen from 0 to 1 V, which coincides with the charge and discharge voltage range. The redox peaks can be easily observed at the slow scan rate, which could be explained by the inserting and blocking of  $\text{Li}^+$  in  $\text{Li}_4\text{Mn}_5\text{O}_{12}$ . The redox reactions could then easily happen at the slow scan rate. At the high scan rates, the redox peaks disappear and the electric polarization appears. This might be because electric polarization becomes serious with the increase of scan rate [2,30]. The integral capacitance is  $147.25 \text{ F g}^{-1}$  at the scan rate of  $2 \text{ mV s}^{-1}$ , and remains at  $31 \text{ F g}^{-1}$  at  $20 \text{ mV s}^{-1}$ , according to Equation (4). Figure 4c shows the charging and discharging curves at different voltages. With the increase of charge–discharge voltage, the discharging time increased gradually, and the curves are parallel and consistent, indicating that this material has good electrochemical performance.

At the same time, we can also observe that at the small current intensity, there will be an obvious discharge platform, which corresponds to the peak appearing at a smaller scanning rate in Figure 4b. Figure 4d reveals the charge–discharge curves of different currents. An obvious internal resistance (IR) drop could be observed from 1 V to 0.9 V in Figure 4d, indicating the existence of the intrinsic resistance of the material itself. Based on the above equations, the waxberry-like nanosphere  $\text{Li}_4\text{Mn}_5\text{O}_{12}$  shows good capacitance; the specific capacitance of waxberry-like nanosphere  $\text{Li}_4\text{Mn}_5\text{O}_{12}$  was about  $535 \text{ mF cm}^{-2}$ , and the energy density was  $110.7 \text{ Wh kg}^{-1}$  when the power density is  $70 \text{ W kg}^{-1}$ . The performance parameter of the waxberry-like nanosphere  $\text{Li}_4\text{Mn}_5\text{O}_{12}$  electrode material has been improved as reported earlier [1,16,21,24,31]. When the charge and discharge current becomes larger, the capacitance of waxberry-like nanosphere  $\text{Li}_4\text{Mn}_5\text{O}_{12}$  becomes smaller. The image also shows that the waxberry-like nanosphere  $\text{Li}_4\text{Mn}_5\text{O}_{12}$  has a charging and discharging platform even at the large current, which indicates that the redox reaction has occurred again during the charge–discharge process. Figure 4e displays the partial charge discharge curve at  $2.5 \text{ mA cm}^{-2}$  in the cyclic charge discharge test. It exhibits the charge discharge stability. Figure 4f shows the lattice structure of  $\text{Li}_4\text{Mn}_5\text{O}_{12}$ . A part of the  $\text{Li}^+$  ions occupies the tetrahedral 8a sites, while the  $\text{Mn}^{4+}$  and the remaining  $\text{Li}^+$  ions are located at octahedral 16d sites with the ratio of 1:5; randomly, the  $\text{O}^{2-}$  ions occupy the sites at 32e. Therefore, the materials can be described as  $[\text{Li}]_{8a}[\text{Li}_{1/3}\text{Mn}_{5/3}]_{16d}[\text{O}_4]_{32e}$  [27].



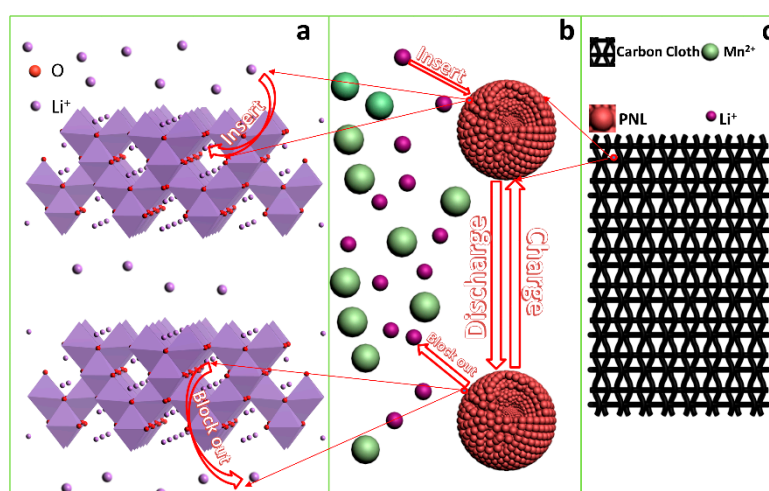
**Figure 4.** (a) The cyclic voltammeter (CV) image of waxberry-like nanosphere  $\text{Li}_4\text{Mn}_5\text{O}_{12}$  in  $1 \text{ mol L}^{-1}$   $\text{LiNO}_3$  electrolyte with the scan rate at  $20 \text{ mV s}^{-1}$  in different potential windows. (b) The CV image of waxberry-like nanosphere  $\text{Li}_4\text{Mn}_5\text{O}_{12}$  in  $1 \text{ mol L}^{-1}$   $\text{LiNO}_3$  electrolyte with different scan rates. (c) The charging and discharging curves at different voltages. (d) The charge–discharge curves at different currents. (e) Charge and discharge curves in cycling test. (f) Lattice structure of  $\text{Li}_4\text{Mn}_5\text{O}_{12}$ .

Figure 5a displays the charge–discharge transport mechanism of waxberry-like nanosphere  $\text{Li}_4\text{Mn}_5\text{O}_{12}$  in  $1 \text{ mol L}^{-1}$   $\text{LiNO}_3$  electrolyte. During the charging process, for the micro mechanism of waxberry-like nanosphere  $\text{Li}_4\text{Mn}_5\text{O}_{12}$ , the  $\text{Li}^+$  ions in the electrolyte are embedded in the lattice of materials. The possible mechanism of this phenomenon can be described as follows [22,32]:



Figure 5b shows the charge–discharge transport mechanism of waxberry-like nanosphere  $\text{Li}_4\text{Mn}_5\text{O}_{12}$  on the atomic scale in  $1 \text{ mol L}^{-1}$   $\text{LiNO}_3$  electrolyte. The  $\text{Li}^+$  ions make contact between the surface of materials and the electrolyte, and the porous structure allows the material to have more contact area with the electrolyte, making the transport process of  $\text{Li}^+$  ion occur more rapidly. Figure 5c reveals the diagram of charge and discharge in macro scale. The carbon cloth has superior electrical

conductivity, which is known to us, making the material adsorbed on the carbon cloth have good stability and conductivity.



**Figure 5.** (a) The charge–discharge transport mechanism of waxberry-like nanosphere  $\text{Li}_4\text{Mn}_5\text{O}_{12}$  on the lattice scale. (b) The charge–discharge transport mechanism of waxberry-like nanosphere  $\text{Li}_4\text{Mn}_5\text{O}_{12}$  on the atomic scale. (c) The diagram of charge and discharge in macro scale.

Figure 6a,b reveals the charge–discharge curves and CV image after being cycled at 1500, 3500, and 5000 times, respectively. The charging time gradually decreased with the increasing of cycle times; at the same time, the discharging time is not obviously shortened, while the initial voltage drop also changed with the discharge process. This may be due to increased contact area between the electrolyte and the internal interface of the waxberry-like nanosphere  $\text{Li}_4\text{Mn}_5\text{O}_{12}$ ; during the activation process of material during charging and discharging during the process listed above, the electrolyte passes through the hole into the waxberry-like nanosphere  $\text{Li}_4\text{Mn}_5\text{O}_{12}$ , which leads to the faster charge time to the expected voltage. The CV of waxberry-like nanosphere  $\text{Li}_4\text{Mn}_5\text{O}_{12}$  showed no obvious change at the cycle process, which confirms its excellent cycle life in  $1 \text{ mol L}^{-1} \text{ LiNO}_3$  solution. The electrochemical impedance spectroscopy (EIS) of waxberry-like nanosphere  $\text{Li}_4\text{Mn}_5\text{O}_{12}$  was displayed in Figure 6c,d, the resistance of the waxberry-like nanosphere  $\text{Li}_4\text{Mn}_5\text{O}_{12}$  increased from the first cycles to the 2000th cycles, with the angle of inclination increasing gradually, and then continued to increase from the 2000th to the 5000th cycle, while at the same time the inclination angle decreased gradually. The EIS shape in the first, 2000th, and 5000th cycles had no significant change, indicating that the ion transport mechanism has not changed much in the charge–discharge process. The decrease in cycles may be due to the reason that besides the redox reaction of lithium ion intercalation, there are a lot of side reactions, such as electrolyte decomposition, dissolution of active substances, and deposition of lithium metal. In the subsequent charge and discharge tests (from 2000th to 5000th), the attenuation of the capacitance is mainly due to the normal capacity attenuation of the material itself.

The reason for the long cycling life of  $\text{Li}_4\text{Mn}_5\text{O}_{12}$  can be explained as follows: (1) the stability of the waxberry-like nano-spherical structural material improves the insertion and blocks the efficiency of  $\text{Li}^+$  ions during the charging and discharging process [33]; (2) proper charging voltage avoids manganese depletion caused by the change of the valence state of manganese [34]. Because of the reasons above, the material has a good stability during the cycling process.

Figure 7a,b shows the comparison of the charge–discharge curves at  $0.25 \text{ mA cm}^{-2}$  and the CV image between raspberry-like nanosphere and waxberry-like nanosphere  $\text{Li}_4\text{Mn}_5\text{O}_{12}$ . The weight of the two samples is both 12 mg. From the CV image, we can see that the area of waxberry-like nanosphere  $\text{Li}_4\text{Mn}_5\text{O}_{12}$  is larger than raspberry-like nanosphere  $\text{Li}_4\text{Mn}_5\text{O}_{12}$ . The charge-discharge time of the former is longer than that of the latter too, which shows that the electrochemical performance of the waxberry-like nanosphere  $\text{Li}_4\text{Mn}_5\text{O}_{12}$  is better than that of the raspberry-like nanosphere

$\text{Li}_4\text{Mn}_5\text{O}_{12}$ . This may be because that the waxberry-like nanosphere material inside the porous sphere can also participate in the reaction. Therefore, in this paper, we chose WLN for a complete study of electrochemical properties. The capacitance of the two samples during charge-discharge cycling at the current at  $2.5 \text{ mA cm}^{-2}$  can be seen in Figure 7c. The capacitance of waxberry-like nanosphere  $\text{Li}_4\text{Mn}_5\text{O}_{12}$  was about  $240 \text{ mF cm}^{-2}$  at the first cycling, decreasing sharply to  $170 \text{ mF cm}^{-2}$  and gradually to  $160 \text{ mF cm}^{-2}$  after 1000 cycles; then, the capacitance remained at  $160 \text{ mF cm}^{-2}$  from the 1000th to the 5000th cycle without obviously decreasing. This may be because the contribution of reactive manganese oxide in the material to the capacitance and the manganese oxide in the electrolyte dissolves rapidly with the charging and discharging process; the capacitance is gradually contributed by lithium manganate, resulting in a rapid drop of capacitive [34]. The cycling stability of raspberry-like nanosphere  $\text{Li}_4\text{Mn}_5\text{O}_{12}$  is almost the same as that of the waxberry-like nanosphere  $\text{Li}_4\text{Mn}_5\text{O}_{12}$ , but its capacitance is lower, which may be the reason that the porous structure of the  $\text{Li}_4\text{Mn}_5\text{O}_{12}$  could allow the electrolyte to have the contact with the inside material; in addition, the hollow structure of nanosphere  $\text{Li}_4\text{Mn}_5\text{O}_{12}$  could not have the same path as the above process. Both of two samples have the good cyclic stability after the 1000th charge–discharge cycle, showing that waxberry-like nanosphere  $\text{Li}_4\text{Mn}_5\text{O}_{12}$  has the better electrochemical performance in the voltage range of 0–1 V.

The electrochemical performance of this work with the other reports are displayed in Table 1. Compared with the other work, Waxberry-like nano porous spinel  $\text{Li}_4\text{Mn}_5\text{O}_{12}$  has the better electrochemical stability and better capacitance performance.

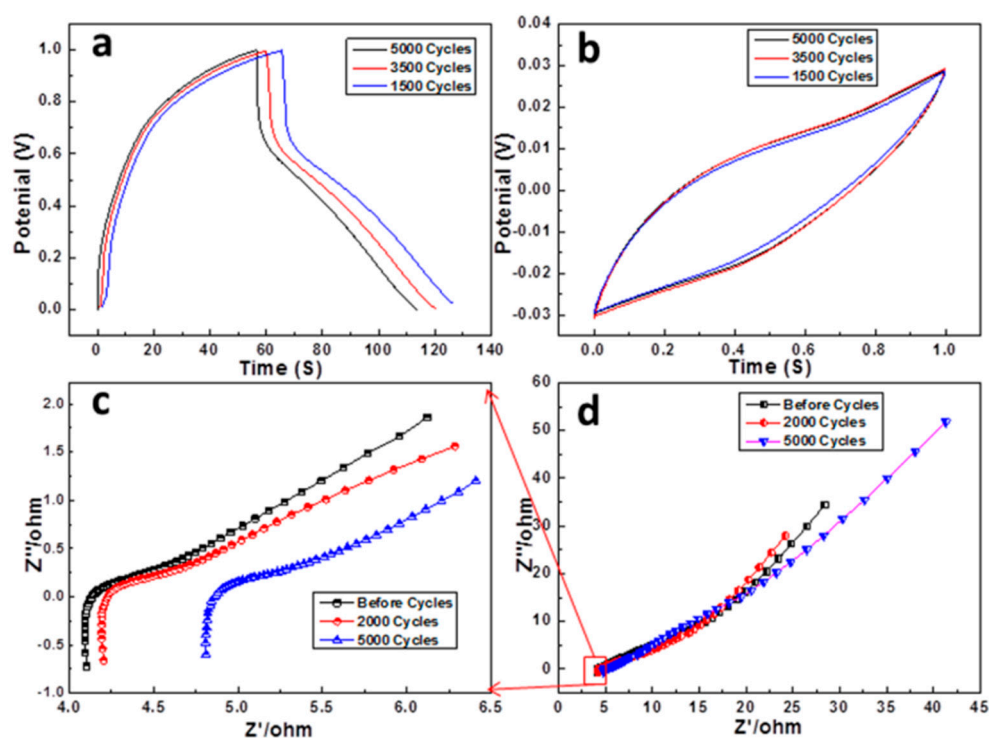


**Figure 6.** (a) The charge–discharge curves after being cycled 1500, 3500, and 5000 times, respectively. (b) The CV image after being cycled 1500, 3500, and 5000 times, respectively. (c,d) The electrochemical impedance spectroscopy (EIS) of waxberry-like nanosphere  $\text{Li}_4\text{Mn}_5\text{O}_{12}$  in the cycling process.

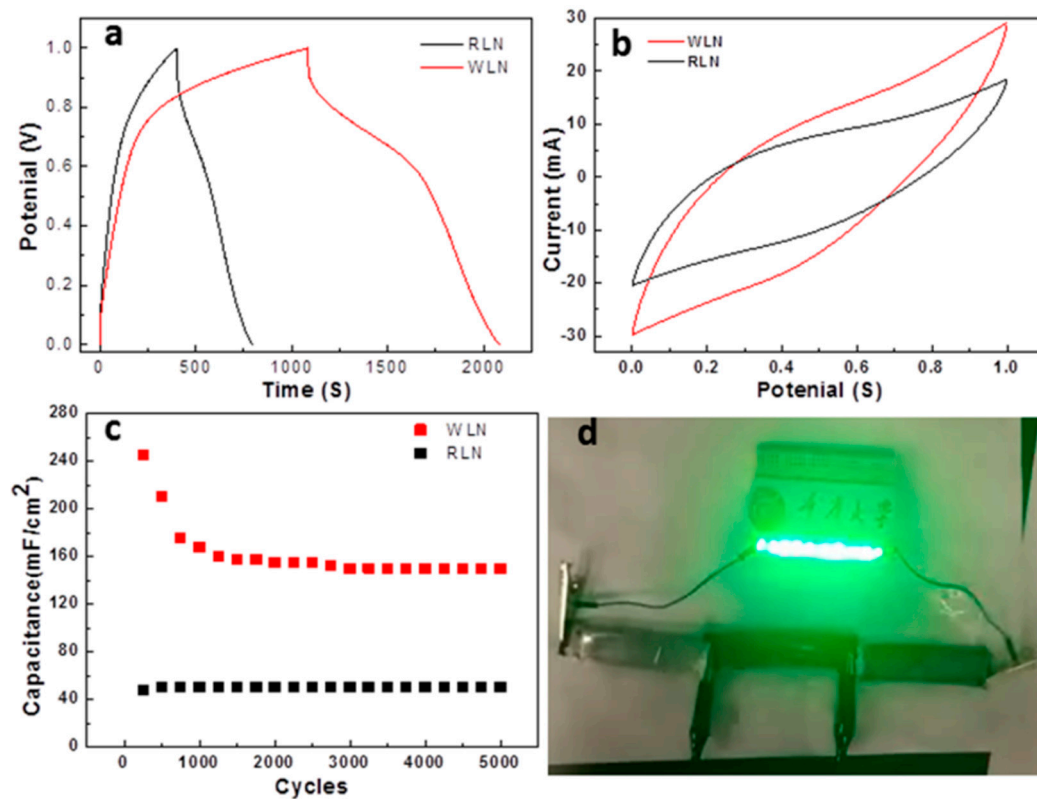


**Figure 7.** The comparison of charge–discharge curves at  $0.25 \text{ mA cm}^{-2}$  (a) and CV curves (b) at  $100 \text{ mV s}^{-1}$  between porous nanosphere and waxberry-like nanosphere  $\text{Li}_4\text{Mn}_5\text{O}_{12}$ . (c) The capacitance of the two samples during charge–discharge cycling at the current at  $2.5 \text{ mA cm}^{-2}$ . (d) The practical application of waxberry-like nanosphere  $\text{Li}_4\text{Mn}_5\text{O}_{12}$  supercapacitors for lighting up ten LEDs.

**Table 1.** Comparison with the work of other reports.

Materials	Capacitance	Scan Rate	Current	Cyclic Stability	Power Density	Energy Density	Reference
Nano crystalline $\text{Li}_4\text{Mn}_5\text{O}_{12}$	$33 \text{ F g}^{-1}$	$2 \text{ mV s}^{-1}$	—	45.5% after 100 cycles	$22.5 \text{ W Kg}^{-1}$	$100 \text{ Wh kg}^{-1}$	[16]
$\text{Li}_4\text{Mn}_5\text{O}_{12}@\text{MnO}_2$	$51.3 \text{ F g}^{-1}$	—	$0.1 \text{ A g}^{-1}$	61.1% after 600 cycles	$43.3 \text{ W kg}^{-1}$	$65 \text{ Wh Kg}^{-1}$	[24]
Waxberry-like nano porous spinel $\text{Li}_4\text{Mn}_5\text{O}_{12}$	$147.25 \text{ F g}^{-1}/535 \text{ mF cm}^{-2}$	$2 \text{ mV s}^{-1}/0.25 \text{ mA cm}^{-2}$	—	70% after 5000 cycles	$70 \text{ W kg}^{-1}$	$110.7 \text{ Wh kg}^{-1}$	This work
Cubic spinel $\text{Li}_4\text{Mn}_5\text{O}_{12}$	$149.5 \text{ F g}^{-1}$	—	$0.2 \text{ A g}^{-1}$	98.2% after 900 cycles	$146.2 \text{ W kg}^{-1}$	$140 \text{ Wh Kg}^{-1}$	[27]

### 3.3. Application

We used three assembled working electrodes ( $6 \text{ cm} \times 2 \text{ cm}$ ) as the power source. After charging at  $10 \text{ mA}$  for  $180 \text{ s}$ , the power source showed good performance in lighting ten LEDs that connected in parallel in the circuit. The working electrode could light ten LEDs for about  $20 \text{ min}$  (Figure 7d and in video). Furthermore, The CV performance of the assembled devices under flexible bending were also tested, as can be seen in Figure S2; with the change of the bending degree of the device, the CV diagram of the supercapacitors did not change significantly, which proves that the device has good flexibility, and for the future application of the device. All those results indicate that this material has the potential to be a power source in the further application.

#### 4. Conclusions

In summary,  $\text{Li}_4\text{Mn}_5\text{O}_{12}$  with the waxberry-like and raspberry-like nanosphere structures were successfully synthesized under the temperature at  $600\text{ }^\circ\text{C}$  by wet chemistry and the template method. Compared with raspberry-like nanosphere structure and previous work,  $\text{Li}_4\text{Mn}_5\text{O}_{12}$  with the waxberry-like nanosphere shows better electrochemical performance (the specific capacitance of  $535\text{ mF cm}^{-2}$  and the energy density of  $110.7\text{ Wh kg}^{-1}$ ) and good stability at room temperature. Moreover, the performance parameter of the waxberry-like nanosphere  $\text{Li}_4\text{Mn}_5\text{O}_{12}$  has been improved as reported earlier [16,24]. All of these results indicate that the waxberry-like nano-porous spinel  $\text{Li}_4\text{Mn}_5\text{O}_{12}$  could provide potential applications in high-performance supercapacitors.

**Supplementary Materials:** The following are available online at <http://www.mdpi.com/2079-9268/8/3/32/s1>.

**Author Contributions:** Experimental design, theoretical calculation and guidance to experimental process: P.J., Y.X., D.Z., C.H. Analyze the experimental data: P.J., C.Z., Y.G. Writing and editing of articles: P.J., Y.X., C.W.

**Funding:** This research received no external funding.

**Acknowledgments:** This work is supported by the National Nature Science Foundation of China (NSFC) (51772036), Natural Science Foundation Project of Chongqing (NSFCQ) (cstc2014jcyjA50030), the graduate scientific research and innovation foundation of Chongqing, China (Grant Nos. CYS16016, CYS17042), NSFC (51572040, 51402112), the Development Program (“863” Program) of China (2015AA034801), the Fundamental Research Funds for the Central Universities (106112015CDJXY300004, 106112017CDJXY300004), the National Key Research and Development Programs—Intergovernmental International Cooperation in Science and Technology Innovation Project (Grant No. 2016YFE0111500), and the large-scale equipment sharing fund of Chongqing University.

**Conflicts of Interest:** The authors declare no conflicts of interest.

#### References

1. Zainol, N.H.; Osman, Z.; Kamarulzaman, N.; Rusdi, R. Investigation on the electrochemical performances of  $\text{Li}_4\text{Mn}_5\text{O}_{12}$  for battery applications. *Ionics* **2016**, *23*, 303–307. [[CrossRef](#)]
2. Qu, Q.; Fu, L.; Zhan, X.; Samuelis, D.; Maier, J.; Li, L.; Tian, S.; Li, Z.; Wu, Y. Porous  $\text{LiMn}_2\text{O}_4$  as cathode material with high power and excellent cycling for aqueous rechargeable lithium batteries. *Energy Environ. Sci.* **2011**, *4*, 3985–3990. [[CrossRef](#)]
3. Zhang, C.; Xi, Y.; Wang, C.; Hu, C.; Liu, Z.; Javed, M.S.; Wang, M.; Lai, M.; Yang, Q.; Zhang, D. High-performance flexible supercapacitors based on  $\text{C}/\text{Na}_2\text{Ti}_5\text{O}_{11}$  nanocomposite electrode materials. *J. Mater. Sci.* **2017**, *52*, 13897–13908. [[CrossRef](#)]
4. Wang, C.; Xi, Y.; Wang, M.; Zhang, C.; Wang, X.; Yang, Q.; Li, W.; Hu, C.; Zhang, D. Carbon-modified  $\text{Na}_2\text{Ti}_3\text{O}_7$  center dot  $2\text{H}_2\text{O}$  nanobelts as redox active materials for high-performance supercapacitor. *Nano Energy* **2016**, *28*, 115–123. [[CrossRef](#)]
5. Mishra, R.K.; Manivannan, S.; Kim, K.; Kwon, H.I.; Jin, S.H. Petal-like  $\text{MoS}_2$  nanostructures with metallic 1T phase for high performance supercapacitors. *Curr. Appl. Phys.* **2018**, *18*, 345–352. [[CrossRef](#)]
6. Wu, C.; Cai, J.; Zhu, Y.; Zhang, K. Hybrid Reduced Graphene Oxide Nanosheet Supported Mn-Ni-Co Ternary Oxides for Aqueous Asymmetric Supercapacitors. *ACS Appl. Mater. Interfaces* **2017**, *9*, 19114–19123. [[CrossRef](#)] [[PubMed](#)]
7. Sim, C.M.; Choi, S.H.; Kang, Y.C. Superior electrochemical properties of  $\text{LiMn}_2\text{O}_4$  yolk-shell powders prepared by a simple spray pyrolysis process. *Chem. Commun. (Camb.)* **2013**, *49*, 5978–5980. [[CrossRef](#)] [[PubMed](#)]
8. Dolphijn, G.; Isikli, S.; Gauthy, F.; Vlad, A.; Gohy, J.F. Hybrid  $\text{LiMn}_2\text{O}_4$ -radical polymer cathodes for pulse power delivery applications. *Electrochim. Acta* **2017**, *255*, 442–448. [[CrossRef](#)]
9. Azari, S.R.; Rahmanifar, M.S.; El-Kady, M.F.; Noori, A.; Mousavi, M.F.; Kaner, R.B. A wide potential window aqueous supercapacitor based on  $\text{LiMn}_2\text{O}_4$ -rGO nanocomposite. *J. Iran. Chem. Soc.* **2017**, *14*, 2579–2590. [[CrossRef](#)]
10. Mao, Y.; Xiao, S.; Liu, J. Nanoparticle-assembled  $\text{LiMn}_2\text{O}_4$  hollow microspheres as high-performance lithium-ion battery cathode. *Mater. Res. Bull.* **2017**, *96*, 437–442. [[CrossRef](#)]

11. Kun, R.; Schlee, P.; Pal, E.; Busse, M.; Gesing, T. Role of the precursor chemistry on the phase composition and electrochemical performance of thin-film  $\text{LiMn}_2\text{O}_4$  Li-ion battery cathodes prepared by spray pyrolysis. *J. Alloys Compd.* **2017**, *726*, 664–674. [[CrossRef](#)]
12. Kim, S.; Aykol, M.; Hegde, V.I.; Lu, Z.; Kirklin, S.; Croy, J.R.; Thackeray, M.M.; Wolverton, C. Material design of high-capacity Li-rich layered-oxide electrodes:  $\text{Li}_2\text{MnO}_3$  and beyond. *Energy Environ. Sci.* **2017**, *10*, 2201–2211. [[CrossRef](#)]
13. Yao, X.; Hu, Y.; Su, Z. Effects of acid treatment on electrochemical properties of  $\text{Li}_2\text{MnO}_3 \cdot \text{LiNi}_{0.5}\text{Co}_{0.45}\text{Fe}_{0.05}\text{O}_2$  cathode materials. *Chem. Pap.* **2017**, *71*, 2465–2471. [[CrossRef](#)]
14. Freire, M.; Lebedev, O.I.; Maignan, A.; Jordy, C.; Pralong, V. Nanostructured  $\text{Li}_2\text{MnO}_3$ : A disordered rock salt type structure for high energy density Li ion batteries. *J. Mater. Chem. A* **2017**, *5*, 21898–21902. [[CrossRef](#)]
15. Kaewmala, S.; Chantrasuwan, P.; Wiriya, N.; Srilomsak, S.; Limphirat, W.; Limthongkul, P.; Meethong, N.  $\text{Li}_2\text{MnO}_3$  domain size and current rate dependence on the electrochemical properties of  $0.5\text{Li}_2\text{MnO}_3 \cdot 0.5\text{LiCoO}_2$  cathode material. *Sci. Rep.* **2017**, *7*, 13196. [[CrossRef](#)] [[PubMed](#)]
16. Tran, V.M.; Huynh, L.T.N.; Ha, C.T.D.; Nguyen, T.M.V.; Le, M.L.P. Electrochemical properties of non-stoichiometric nanocrystalline  $\text{Li}_4\text{Mn}_5\text{O}_{12}$  for hybrid capacitors. *Adv. Nat. Sci. Nanosci. Nanotechnol.* **2016**, *7*, 015012.
17. Zhou, L.; Zhou, X.; Huang, X.; Liu, Z.; Zhao, D.; Yao, X.; Yu, C. Designed synthesis of  $\text{LiMn}_2\text{O}_4$  microspheres with adjustable hollow structures for lithium-ion battery applications. *J. Mater. Chem. A* **2013**, *1*, 837–842. [[CrossRef](#)]
18. Xie, A.; Tao, F.; Jiang, C.; Sun, W.; Li, Y.; Hu, L.; Du, X.; Luo, S.; Yao, C. A coralliform-structured  $\gamma\text{-MnO}_2$  /polyaniline nanocomposite for high-performance supercapacitors. *J. Electroanal. Chem.* **2017**, *789*, 29–37. [[CrossRef](#)]
19. Javed, M.S.; Dai, S.; Wang, M.; Guo, D.; Chen, L.; Wang, X.; Hu, C.; Xi, Y. High performance solid state flexible supercapacitor based on molybdenum sulfide hierarchical nanospheres. *J. Power Sources* **2015**, *285*, 63–69. [[CrossRef](#)]
20. Dai, S.; Xi, Y.; Hu, C.; Liu, J.; Zhang, K.; Yue, X.; Cheng, L.  $\text{KCu}_7\text{S}_4$  nanowires and the  $\text{Mn}/\text{KCu}_7\text{S}_4$  nanostructure for solid-state supercapacitors. *J. Mater. Chem. A* **2013**, *1*, 15530. [[CrossRef](#)]
21. Tian, Y.; Chen, D.; Jiao, X.; Duan, Y. Facile preparation and electrochemical properties of cubic-phase  $\text{Li}_4\text{Mn}_5\text{O}_{12}$  nanowires. *Chem. Commun.* **2007**, 2072–2074. [[CrossRef](#)]
22. Zhao, Y.; Lai, Q.; Zeng, H.; Hao, Y.; Lin, Z.  $\text{Li}_4\text{Mn}_5\text{O}_{12}$  prepared using l-lysine as additive and its electrochemical performance. *Ionics* **2013**, *19*, 1483–1487. [[CrossRef](#)]
23. Singh, I.B.; Singh, A. A facile low-temperature synthesis of  $\text{Li}_4\text{Mn}_5\text{O}_{12}$  nanorods. *Colloid Polym. Sci.* **2017**, *295*, 689–693. [[CrossRef](#)]
24. Chu, H.Y.; Lai, Q.Y.; Hao, Y.J.; Zhao, Y.; Xu, X.Y. Study of electrochemical properties and the charge/discharge mechanism for  $\text{Li}_4\text{Mn}_5\text{O}_{12}/\text{MnO}_2\text{-AC}$  hybrid supercapacitor. *J. Appl. Electrochem.* **2009**, *39*, 2007–2013. [[CrossRef](#)]
25. Kim, H.U.; Sun, Y.K.; Lee, B.S.; Jin, C.S.; Shin, K.H. Synthesis of Defective-Structure  $\text{Li}_4\text{Mn}_5\text{O}_{12}$  by Combustion Method and Its Application to Hybrid Capacitor. *J. Korean Electrochem. Soc.* **2010**, *13*, 103–109. [[CrossRef](#)]
26. Liu, M.; Zhang, G.J.; Shen, Z.R.; Sun, P.C.; Ding, D.T.; Chen, T.H. Synthesis and characterization of hierarchically structured mesoporous  $\text{MnO}_2$  and  $\text{Mn}_2\text{O}_3$ . *Solid State Sci.* **2009**, *11*, 118–128. [[CrossRef](#)]
27. Hao, Y.J.; Lai, Q.Y.; Xu, X.Y.; Wang, L. Electrochemical performance of symmetric supercapacitor based on  $\text{Li}_4\text{Mn}_5\text{O}_{12}$  electrode in  $\text{Li}_2\text{SO}_4$  electrolyte. *Mater. Chem. Phys.* **2011**, *126*, 432–436. [[CrossRef](#)]
28. Dai, S.; Guo, H.; Wang, M.; Liu, J.; Wang, G.; Hu, C.; Xi, Y. A Flexible micro-supercapacitor based on a pen ink-carbon fiber thread. *J. Mater. Chem. A* **2014**, *2*, 19665–19669. [[CrossRef](#)]
29. Allagui, A.; Freeborn, T.J.; Elwakil, A.S.; Maundy, B.J. Reevaluation of Performance of Electric Double-layer Capacitors from Constant-current Charge/Discharge and Cyclic Voltammetry. *Sci. Rep.* **2016**, *6*, 38568. [[CrossRef](#)] [[PubMed](#)]
30. Zhang, C.; Guo, C.; Li, T.; Ren, X.; Mao, Y.; Wei, Y.; Hou, L. Doping Ni: An effective strategy enhancing electrochemical performance of  $\text{MnCO}_3$  electrode materials for supercapacitors. *J. Mater. Sci.* **2016**, *52*, 1477–1485. [[CrossRef](#)]
31. Fu, Y.; Jiang, H.; Hu, Y.; Zhang, L.; Li, C. Hierarchical porous  $\text{Li}_4\text{Mn}_5\text{O}_{12}$  nano/micro structure as superior cathode materials for Li-ion batteries. *J. Power Sources* **2014**, *261*, 306–310. [[CrossRef](#)]

32. Hao, Y.J.; Wang, Y.Y.; Lai, Q.Y.; Zhao, Y.; Chen, L.M.; Ji, X.Y. Study of capacitive properties for LT-Li<sub>4</sub>Mn<sub>5</sub>O<sub>12</sub> in hybrid supercapacitor. *J. Solid State Electrochem.* **2008**, *13*, 905–912. [[CrossRef](#)]
33. Wang, F.X.; Xiao, S.Y.; Zhu, Y.S.; Chang, Z.; Hu, C.L.; Wu, Y.P.; Holze, R. Spinel LiMn<sub>2</sub>O<sub>4</sub> nanohybrid as high capacitance positive electrode material for supercapacitors. *J. Power Sources* **2014**, *246*, 19–23. [[CrossRef](#)]
34. Chen, Z.; Zhao, Y.; Ma, J.; Liu, C.; Ma, Y. Detailed XPS analysis and anomalous variation of chemical state for Mn- and V-doped TiO<sub>2</sub> coated on magnetic particles. *Ceram. Int.* **2017**, *43*, 16763–16772. [[CrossRef](#)]



© 2018 by the authors. Licensee MDPI, Basel, Switzerland. This article is an open access article distributed under the terms and conditions of the Creative Commons Attribution (CC BY) license (<http://creativecommons.org/licenses/by/4.0/>).